Trajectory control method for hex-rotor UAV

Konstantin Lelkov*

Department of Automated Complexes of Orientation and Navigation Systems, Moscow Aviation Institute (National Research University), 125993, Moscow, Russia

Abstract. A novel approach to the trajectory control system for a hex-rotor unmanned aerial vehicle is proposed. This approach is based on combining existing techniques, such as PID regulators and backstepping control to achieve better control quality in tight-spaced environments. The provided simulation results prove that this approach allows unmanned aerial vehicle to traverse the given trajectory with small offset errors.

1 Introduction

Unmanned Aerial Vehicles (UAVs) have gained significant popularity in various applications, ranging from military surveillance to agricultural monitoring. Among the different types of UAVs, hex-rotor UAVs have emerged as a promising platform due to their enhanced stability, maneuverability, and payload capacity. The control of hex-rotor UAVs plays a crucial role in ensuring their safe and efficient operation in diverse environments.

In recent years, significant advancements have been made in the field of hex-rotor UAV control methods, with researchers exploring innovative techniques to enhance the performance and autonomy of these aerial vehicles [1,2]. The common control approaches are based on either PID controllers, LQR, or MPC methods. However, while these approaches solve the general case of UAV control, they are not applicable for trajectory control (while MPC can actually be used for controlling the UAV's motion along the given trajectory, it requires a detailed model of the vehicle's surroundings, which is not always possible). Trajectory control systems are required to ensure safe operation of the aircraft in tight-spaced environments where deviation from a given trajectory is not allowed.

The primary focus of this paper is to introduce a novel trajectory control method specifically designed for hex-rotor UAVs based on combining existing techniques such as PID control and backstepping control [3,4]. This new approach aims to minimize trajectory offset during the aircraft's flight, particularly in constrained environments where precise trajectory following is critical. By addressing this gap in existing research, this paper contributes to advancing the field of hex-rotor UAV control methods and opens up new possibilities for enhancing the safety and efficiency of these aerial vehicles in challenging operational scenarios.

* Corresponding author: kon.lelkov@gmail.com

2 Hex-rotor dynamics

Prior to developing a control method, the hex-rotor dynamic model should be introduced. There are a number of hex-rotor mathematical models with varying degrees of detail. For this article, we will use the model proposed in the previous research that takes into account such factors as the gyroscopic torque generated by rotation of the rotors and the loss in thrust with the increase in axial velocity across the rotor disk [5, 6].

We will adopt the coordinate frames used in [5, 7]: the body-fixed frame (BFF) attached to the center of mass of the aircraft and the inertial earth-fixed frame (EFF), which is located at the fixed point on the ground. The orientation of both frames follows the NED pattern [8]. The axis $O_E X_E$ aligns with the north direction, and the axis $O_E Y_E$ points to the east. The remaining axis $O_E Z_E$ points straight down, aligning with the gravity vector $\mathbf{g}$. In the BFF, $O_B X_B$ is the longitudinal axis of the vehicle, and $O_B Y_B$ is the lateral one (Fig. 1). For this article, we will assume that the UAV flight distances are small enough to ignore the curvature if the Earth's surface.

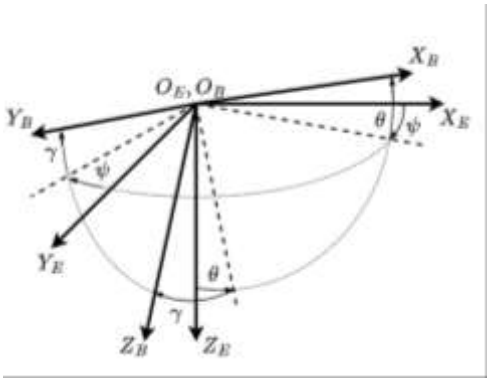

Fig. 1. The rotation from EFF to BFF

The full mathematical model of the hex-rotor aircraft is described in BFF (Fig. 2).

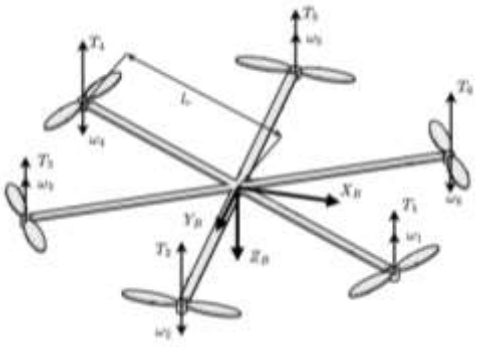

Fig. 2. Hex-rotor frame, directions of thrust vectors and rotation of the motors.

While it is helpful for understanding the effects of the forces on the aircraft's body, it is not convenient for developing a trajectory control system. In general, the given trajectory of UAV flight is given relative to the position of the observer or real-world objects (structures, tunnels, etc.). This is why the dynamic model of the hex-rotor should be rewritten in EFF:

$$
\begin{aligned}
&m_a\ddot{x}_a = -\sum_1^6 T_i\left(\sin\psi\sin\gamma+\cos\psi\sin\theta\cos\gamma\right)+\frac{1}{2}\rho C_{Tx}S_x W_a^{\,2}\cos\psi\cos\theta+m_a\left(\dot{\theta}\dot{z}_a-\dot{y}_a\dot{\psi}\right)+\\
&+\frac{1}{2}\rho C_{Ty}S_y W_a^{\,2}\left(\cos\psi\sin\theta\sin\gamma-\sin\psi\cos\gamma\right)+\frac{1}{2}\rho C_{Tz}S_z W_a^{\,2}\left(\cos\psi\sin\theta\cos\gamma+\sin\psi\sin\gamma\right);\\
&m_a\ddot{y}_a = \sum_1^6 T_i\left(\cos\psi\sin\gamma-\sin\psi\sin\theta\cos\gamma\right)+\frac{1}{2}\rho C_{Tx}S_x W_a^{\,2}\sin\psi\cos\theta+m_a\left(\dot{\gamma}\dot{z}_a-\dot{x}_a\dot{\psi}\right)+\\
&+\frac{1}{2}\rho C_{Ty}S_y W_a^{\,2}\left(\cos\psi\cos\gamma+\sin\psi\sin\theta\sin\gamma\right)+\frac{1}{2}\rho C_{Tz}S_z W_a^{\,2}\left(\sin\psi\sin\theta\cos\gamma-\cos\psi\sin\gamma\right);\\
&m_a\ddot{z}_a = m_a g-\sum_1^6 T_i\cos\theta\cos\gamma-\frac{1}{2}\rho C_{Tx}S_x W_a^{\,2}\sin\theta+\frac{1}{2}\rho C_{Ty}S_y W_a^{\,2}\cos\theta\sin\gamma+\\
&+\frac{1}{2}\rho C_{Tz}S_z W_a^{\,2}\cos\theta\cos\gamma+m_a\left(\dot{\theta}\dot{x}_a-\dot{\gamma}\dot{y}_a\right);\\
&I_{az}\ddot{\psi} = k_r\left(T_1-T_2+T_3-T_4+T_5-T_6\right)+\dot{\gamma}\dot{\theta}\left(I_{ax}-I_{ay}\right)+\frac{1}{2}\rho C_{Rz}S_a l_r W_a^{\,2};\\
&I_{ay}\ddot{\theta} = \frac{\sqrt{3}}{2}l_r\left(T_1-T_3-T_4+T_6\right)+\dot{\psi}\dot{\gamma}\left(I_{az}-I_{ax}\right)+\frac{\sqrt{3}}{4}\rho C_{Ry}S_a l_r W_a^{\,2}-I_R\dot{\gamma}G_r;\\
&I_{ax}\ddot{\gamma} = \frac{\sqrt{3}}{2}l_r\left(T_6+T_4-T_3-T_1\right)+l_r\left(T_5-T_2\right)+\dot{\theta}\dot{\psi}\left(I_{ay}-I_{az}\right)+\frac{1}{2}\rho C_{Rx}S_a l_r W_a^{\,2}+I_R\dot{\theta}G_r.
\end{aligned}
\tag{1}
$$

In these equations, the following notations are used: m_a – UAV's mass; x_a, y_a, z_a – UAV coordinates in EFF; ψ, θ, γ – heading, pitch, and roll angles, respectively; W_a – airspeed; $T_1 ... T_6$ – thrust value of the respective motors; g – gravity acceleration; ρ – air density; $G_r = -\omega_1 + \omega_2 - \omega_3 + \omega_4 - \omega_5 + \omega_6$, where $\omega_1 ... \omega_6$ is the rotation rate of the respective motor; C_{Tx}, C_{Ty}, C_{Tz} – parameters of aerodynamic forces acting on the aircraft; C_{Rx}, C_{Ry}, C_{Rz} – parameters of aerodynamic moments acting on the aircraft; S_x, S_y, S_z – UAV areas in respective directions of BFF; l_r – linear displacement of the motor from the center of mass; S_a – aerodynamic area; I_{ax}, I_{ay}, I_{az} – components of the inertia tensor.

For simplification, we will rewrite the equations (1) in vector form. First, we define the state vector of the system that contains all the parameters we eventually want to control:

$$
X_a = \left[x_a, \dot{x}_a, y_a, \dot{y}_a, z_a, \dot{z}_a, \psi, \dot{\psi}, \theta, \dot{\theta}, \gamma, \dot{\gamma}\right]^T \tag{2}
$$

Then we define the control vector, containing the thrust values of each rotor:

$$
U = \begin{bmatrix} U_1 \\ U_2 \\ U_3 \\ U_4 \end{bmatrix} = \begin{bmatrix} T_1+T_2+T_3+T_4+T_5+T_6 \\ k_r\left(T_1-T_2+T_3-T_4+T_5-T_6\right) \\ \frac{\sqrt{3}}{2}l_r\left(T_1-T_3-T_4+T_6\right) \\ \frac{\sqrt{3}}{2}l_r\left(T_6+T_4-T_3-T_1\right)+l_r\left(T_5-T_2\right) \end{bmatrix} \tag{3}
$$

The component U_1 describes lift force control channel, while the components U_2, U_3, U_4 describe heading, pitch, and roll channels, respectively.

And the aerodynamic vector, which includes all the aerodynamic forces and moments:

$$A = \left[A_1, A_2, A_3, A_4, A_5, A_6 \right]^T , \tag{4}$$

where:

$$A_1 = \frac{1}{2}\rho C_{Tx} S_x W_a^2 \cos\psi \cos\theta + \frac{1}{2}\rho C_{Ty} S_y W_a^2 \left(\cos\psi \sin\theta \sin\gamma - \sin\psi \cos\gamma\right) +$$

$$+\frac{1}{2}\rho C_{Tz} S_z W_a^2 \left(\cos\psi \sin\theta \cos\gamma + \sin\psi \sin\gamma\right);$$

$$A_2 = \frac{1}{2}\rho C_{Tx} S_x W_a^2 \sin\psi \cos\theta + \frac{1}{2}\rho C_{Ty} S_y W_a^2 \left(\cos\psi \cos\gamma + \sin\psi \sin\theta \sin\gamma\right) +$$

$$+\frac{1}{2}\rho C_{Tz} S_z W_a^2 \left(\sin\psi \sin\theta \cos\gamma - \cos\psi \sin\gamma\right);$$

$$A_3 = -\frac{1}{2}\rho C_{Tx} S_x W_a^2 \sin\theta + \frac{1}{2}\rho C_{Ty} S_y W_a^2 \cos\theta \sin\gamma + \frac{1}{2}\rho C_{Tz} S_z W_a^2 \cos\theta \cos\gamma;$$

$$A_4 = \frac{1}{2}\rho C_{Rz} S_a l_r W_a^2;$$

$$A_5 = \frac{\sqrt{3}}{4}\rho C_{Ry} S_a l_r W_a^2;$$

$$A_6 = \frac{1}{2}\rho C_{Rx} S_a l_r W_a^2.$$

Now we can rewrite the dynamic system (1) in its state-space representation form:

$$\dot{x}_1 = x_2;$$

$$\dot{x}_2 = -\frac{U_1}{m_a}\left(\sin x_7 \sin x_{11} + \cos x_7 \sin x_9 \cos x_{11}\right) + \frac{A_1}{m_a} + \left(x_{10} x_6 - x_4 x_8\right);$$

$$\dot{x}_3 = x_4;$$

$$\dot{x}_4 = \frac{U_1}{m_a}\left(\cos x_7 \sin x_{11} - \sin x_7 \sin x_9 \cos x_{11}\right) + \frac{A_2}{m_a} + \left(x_{12} x_6 - x_2 x_8\right);$$

$$\dot{x}_5 = x_6;$$

$$\dot{x}_6 = g - \frac{U_1}{m_a}\cos x_9 \cos x_{11} + \frac{A_3}{m_a} + \left(x_{10} x_2 - x_{12} x_4\right);$$

$$\dot{x}_7 = x_8;$$

$$\dot{x}_8 = \frac{1}{I_{az}} U_2 + \frac{A_4}{I_{az}} + x_{12} x_{10} \left(\frac{I_{ax} - I_{ay}}{I_{az}}\right);$$

$$\dot{x}_9 = x_{10};$$

$$\dot{x}_{10} = \frac{1}{I_{ay}} U_3 + \frac{A_5}{I_{ay}} + x_8 x_{12} \left(\frac{I_{az} - I_{ax}}{I_{ay}}\right) - \frac{I_R}{I_{ay}} x_{12} G_r;$$

$$\dot{x}_{11} = x_{12};$$

$$\dot{x}_{12} = \frac{1}{I_{ax}} U_4 + \frac{A_6}{I_{ax}} + x_{10} x_8 \left(\frac{I_{ay} - I_{az}}{I_{ax}}\right) + \frac{I_R}{I_{ay}} x_{10} G_r. \tag{5}$$

These equations describe the full mathematical model of the hex-rotor aircraft in EFF.

3 Control method

In order to achieve high-quality trajectory control, a few assumptions are introduced:

- Since the hex-rotor dynamic varies based on the construction axis, the control system can limit the UAV's velocity in order to maintain a low trajectory offset (for example, when the UAV's dynamic along $O_B Z_B$ axis is much higher compared to other BFF axes, the control system might limit the vertical velocity to reduce the trajectory offset).
- The control system can limit the UAV's maneuverability, but it should not limit its degrees of motion.
- The UAV is controlled in "headless" mode – it does not need to make heading rotations to change the direction of motion (heading control is separate from linear motion control).
- The trajectory offset during hex-rotor flight should be lower than 1.5 meters.
- The control system should provide means to control the UAV's position as well as its velocities.
- The trajectory is given in the form of subsequent waypoints (x, y, H, ψ) with three linear coordinates and one angular – heading orientation.

Given the assumptions above, the following control system structure was introduced (Fig. 3).

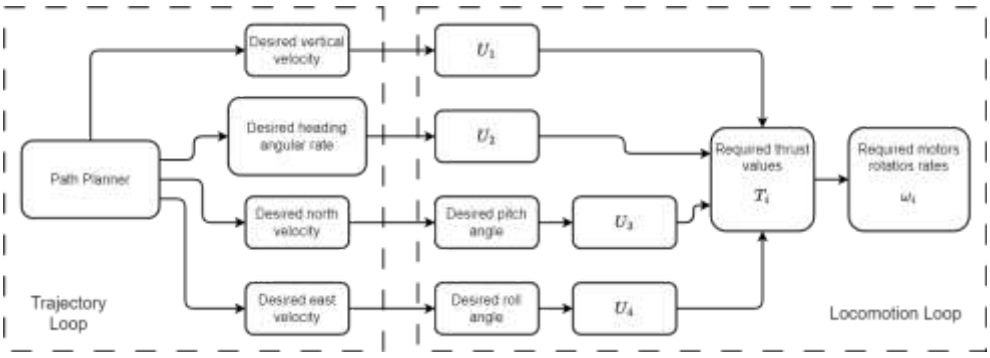

Fig. 3. The structure of the UAV trajectory control system.

This system includes two major control loops: trajectory and locomotion control. While the trajectory control loop is used to control the UAV's motion relative to the given trajectory, the locomotion control loop is used to stabilize the UAV's motion at given velocities.

3.1 Trajectory control loop

The trajectory control loop generates the linear velocity values required to stay "on path" with the given trajectory, as well as the required heading angular rate to maintain the given heading angle. Desired velocities $\dot{x}_d, \dot{y}_d, \dot{z}_d, \dot{\psi}_d$ are generated as an output of the PD regulators [9]:

$$\begin{aligned}
\dot{x}_d &= k_{px} e_x - k_{dx} \frac{de_x}{dt}; \\
\dot{y}_d &= k_{py} e_y - k_{dy} \frac{de_y}{dt}; \\
\dot{z}_d &= k_{pz} e_z - k_{dz} \frac{de_z}{dt}; \\
\dot{\psi}_d &= k_{ph} e_\psi - k_{dh} \frac{de_\psi}{dt},
\end{aligned} \tag{6}$$

where: $e_x = x_{goal} - x_a$; $e_y = y_{goal} - y_a$; $e_z = z_{goal} - z_a$; $e_\psi = \psi_{goal} - \psi$; $x_{goal}, y_{goal}, z_{goal}, \psi_{goal}$ – are the trajectory control goals (waypoint parameters); $k_{px}, k_{py}, k_{pz}, k_{ph}, k_{dx}, k_{dy}, k_{dz}, k_{dh}$ – are constant control coefficients.

The outputs of these PD controllers should be restricted however, since the vertical velocity increases much faster than the horizontal ones. One way to apply the restrictions is to use relative velocities:

$$\begin{aligned}
\left|\dot{x}_d\right| &\le \frac{L_x}{L}; \\
\left|\dot{y}_d\right| &\le \frac{L_y}{L}; \\
\left|\dot{z}_d\right| &\le \frac{L_z}{L},
\end{aligned} \tag{7}$$

where L is the length of the vector connecting the previous waypoint with the current one and L_x, L_y, L_z are the projections of this vector on EFF axes.

Equations (7) restrict only the upper velocity limit, allowing its values to decrease later on so the UAV can reach the given waypoint without overshooting.

Generated values serve as the inputs for the locomotion control loop.

3.2 Locomotion control loop

The main objective of the locomotion control loop is to ensure the asymptotic convergence of the state vector (2) to the desired velocities $\dot{x}_d, \dot{y}_d, \dot{z}_d, \dot{\psi}_d$. For this purpose, we will use backstepping Kokotovich control approach, as described in [10]. The idea of this recursive Lyapunov-bases control loop structure is to design a controller recursively. In this structure, some of the state variables are used as "virtual inputs" for other controller layers.

First, let us define the velocity error along $O_E X_E$ axis as z_2:

$$z_2 = x_{2d} - x_2 \tag{8}$$

The derivative of this velocity error takes form:

$$\dot{z}_2 = \dot{x}_{2d} - \dot{x}_2 \tag{9}$$

To achieve the velocity convergence to the desired value through acceleration $\dot{z}_2$ we add the integral component $k_2 z_2$ to (9) as follows:

$$\dot{z}_2 = \dot{x}_{2d} - \dot{x}_2 + k_2 z_2 \tag{10}$$

where k_2 is a positive coefficient.

Taking into account equation for $\dot{x}_2$ from (5), we can transform the equation (10):

$$\dot{z}_2 = \dot{x}_{2d} + \frac{U_1}{m_a}\left(\sin x_7 \sin x_{11} + \cos x_7 \sin x_9 \cos x_{11}\right) - \frac{A_1}{m_a} - \left(x_{10}x_6 - x_4 x_8\right) + k_2 z_2; \tag{11}$$

To achieve asymptotically stable control, we introduce the Lyapunov function-candidate as follows:

$$\begin{aligned} V_2 &= \frac{1}{2} z_2^2 > 0; \\ \dot{V}_2 &= z_2 \dot{z}_2 \le 0. \end{aligned} \tag{12}$$

The first inequality is always true, but the second one is not defined yet. After substituting equation (11), the second inequality takes form:

$$\dot{V}_2 = z_2\left(\dot{x}_{2d} + \frac{U_1}{m_a}\left(\sin x_7 \sin x_{11} + \cos x_7 \sin x_9 \cos x_{11}\right) - \frac{A_1}{m_a} - \left(x_{10}x_6 - x_4 x_8\right) + k_2 z_2\right) \tag{13}$$

It is easy to see, that in order to meet the asymptotic convergence criteria, $\dot{V}_2$ must be equal to zero. There are two ways to achieve that: if $z_2 = 0$ or the bracket ($\dot{z}_2$) is equal to zero. If z_2 is equal to zero, the control objective is already reached, and further calculations are not required. If $z_2 \neq 0$, the convergence criteria transforms to:

$$\dot{x}_{2d} + \frac{U_1}{m_a}\left(\sin x_7 \sin x_{11} + \cos x_7 \sin x_9 \cos x_{11}\right) - \frac{A_1}{m_a} - \left(x_{10}x_6 - x_4 x_8\right) + k_2 z_2 = 0 \tag{14}$$

Then we introduce virtual control $u_x^* = \left(\sin x_7 \sin x_{11} + \cos x_7 \sin x_9 \cos x_{11}\right)$ and derive it from (14):

$$u_x^* = \frac{m_a}{U_1}\left[\frac{A_1}{m_a} + \left(x_{10}x_6 - x_4 x_8\right) - k_2 z_2\right] \tag{15}$$

Stable flight with the desired velocity can only be achieved if the UAV's acceleration is equal to zero. Hence, we can assume that the component $\dot{x}_{2d} = 0$. To improve the quality of control, we add the dampening component $n_2 \dot{z}_2$ to (15) as follows:

$$u_x^* = \frac{m_a}{U_1}\left[\frac{A_1}{m_a} + \left(x_{10}x_6 - x_4 x_8\right) - k_2 z_2 + n_2 \dot{z}_2\right] \tag{16}$$

where n_2 is a positive coefficient.

Since u_x^* is the orientation variable, it is possible to obtain the desired pitch angle from (14). In order to reach the desired velocity x_{2d}, this angle is given by:

$$x_{9d} = \arcsin\left(\frac{u_x^* - \sin x_7 \sin x_{11}}{\cos x_7 \cos x_{11}}\right) = \arcsin\left(\frac{u_x^* - \sin\psi \sin\gamma}{\cos\psi \cos\gamma}\right) \tag{17}$$

The desired pitch angle x_{9d} is then used as a virtual input for the pitch control channel U_3. First, let us define the pitch angle error and its derivative as follows:

$$\begin{aligned} z_9 &= x_{9d} - x_9; \\ \dot{z}_9 &= \dot{x}_{9d} - x_{10}. \end{aligned} \tag{18}$$

Our control objective is to derive a virtual control x_{10}^* for pitch rotation rate, which achieves $\lim_{t\to\infty} z_9 \to 0$. We pick a Lyapunov function-candidate in such a form, that it always has a positive value:

$$V_9 = \frac{1}{2} z_9^2 > 0 \tag{19}$$

The derivative of this function is:

$$\dot{V}_9 = z_9 \dot{z}_9 = z_9 \left(\dot{x}_{9d} - x_{10}\right) \tag{20}$$

Then we introduce the virtual control x_{10}^* as follows:

$$x_{10}^* = \dot{x}_{9d} + k_9 z_9 \tag{21}$$

where k_9 is a positive coefficient.

Now, the pitch rotation rate error takes form:

$$\begin{aligned} z_{10} &= x_{10}^* - x_{10} = \dot{x}_{9d} + k_9 z_9 - x_{10}; \\ x_{10} &= \dot{x}_{9d} + k_9 z - z_{10}. \end{aligned} \tag{22}$$

In order to achieve stability of the control system $\dot{V}_9$ must be non-positive. Substituting (22) into (20), we get:

$$\dot{V}_9 = z_9 \left(z_{10} - k_9 z_9\right) = z_9 z_{10} - k_9 z_9^2 \le 0 \tag{23}$$

Hence, we can povide $\lim_{t\to\infty} z_9 \to 0$ by satisfying the inequality:

$$z_9 z_{10} \le k_9 z_9^2 \tag{24}$$

Considering the equations (5), the derivative of (22) is as follows:

$$\dot{z}_{10} = \ddot{x}_{9d} + k_9 \dot{z}_9 - \frac{1}{I_{ay}} U_3 - \frac{A_5}{I_{ay}} - x_8 x_{12} \left(\frac{I_{az} - I_{ax}}{I_{ay}}\right) + \frac{I_R}{I_{ay}} x_{12} G_r \tag{25}$$

Then, to achieve stable UAV's orientation control ($\lim_{t\to\infty} z_{10} \to 0$) we will pick another Lyapunov function-candidate:

$$V_{10} = V_9 + \frac{1}{2} z_{10}^2 > 0 \tag{26}$$

It is easy to see that V_{10} is always positive. And for asymptotic convergence of the UAV's pitch rotation rate to the virtual control x_{10}^* the derivative of (26) should always be non-positive:

$$\dot{V}_{10} = \dot{V}_9 + z_{10}\dot{z}_{10} \le 0 \tag{27}$$

Substituting (25) to (27), we get:

$$\dot{V}_{10} = \dot{V}_9 + z_{10}\left(\ddot{x}_{9d} + k_9\dot{z}_9 - \frac{1}{I_{ay}}U_3 - \frac{A_5}{I_{ay}} - x_8x_{12}\left(\frac{I_{az}-I_{ax}}{I_{ay}}\right) + \frac{I_R}{I_{ay}}x_{12}G_r \right). \tag{28}$$

Taking into account (23), equation (28) can be rewritten as follows:

$$\dot{V}_{10} = -k_9z_9^2 + z_{10}\left(z_9 + \ddot{x}_{9d} + k_9\dot{z}_9 - \frac{1}{I_{ay}}U_3 - \frac{A_5}{I_{ay}} - x_8x_{12}\left(\frac{I_{az}-I_{ax}}{I_{ay}}\right) + \frac{I_R}{I_{ay}}x_{12}G_r \right). \tag{29}$$

The stability of this system can be provided by satisfying the following conditions:

$$\begin{cases} -k_9z_9^2 \le 0; \\ z_9 + \ddot{x}_{9d} + k_9\dot{z}_9 - \frac{1}{I_{ay}}U_3 - \frac{A_5}{I_{ay}} - x_8x_{12}\left(\frac{I_{az}-I_{ax}}{I_{ay}}\right) + \frac{I_R}{I_{ay}}x_{12}G_r = 0. \end{cases} \tag{30}$$

Following the same logic we applied for (16), to improve the quality of control, we can drop $\ddot{x}_{9d}$ component and add dampening $k_{10}z_{10}$. In this case, conditions (30) take the following form:

$$\begin{cases} -k_9z_9^2 + k_{10}z_{10}^2 \le 0; \\ z_9 + k_9\dot{z}_9 - \frac{1}{I_{ay}}U_3 - \frac{A_5}{I_{ay}} - x_8x_{12}\left(\frac{I_{az}-I_{ax}}{I_{ay}}\right) + \frac{I_R}{I_{ay}}x_{12}G_r + k_{10}z_{10} = 0. \end{cases} \tag{31}$$

It is easy to see that in order to satisfy these conditions, k_{10} must be negative. Then the control input U_3 can be derived from (31) as follows:

$$U_3 = I_{ay}z_9 + I_{ay}k_9\dot{z}_9 - A_5 - x_8x_{12}\left(I_{az}-I_{ax}\right) + I_Rx_{12}G_r + I_{ay}k_{10}z_{10}. \tag{32}$$

The same procedure can be used to obtain control inputs U_1, U_2, U_4. To maintain the presentation clarity of this paper, we will present only the final equations:

$$
\begin{aligned}
U_1 &= \frac{m_a}{\cos x_9 \cos x_{11}}\left(g + \frac{A_3}{m_a} + \left(x_{10}x_2 - x_{12}x_4\right) - k_6 z_6\right);\\
U_2 &= I_{az} z_7 + I_{az} k_7 \dot{z}_7 - A_4 - x_{12}x_{10}\left(I_{ax} - I_{ay}\right) + I_{az} k_8 z_8;\\
U_4 &= I_{ax}\left(z_{11} + k_{11}\dot{z}_{11} - x_{10}x_8 \frac{I_{ay} - I_{az}}{I_{ax}} - \frac{A_6}{I_{ax}} - \frac{I_R}{I_{ax}} x_{10} G_r + k_{12} z_{12}\right).
\end{aligned}
\tag{33}
$$

The equations (32), (33) allow us to generate the control vector (3). The next step would be to calculate thrust values T1-T6. This cannot be done directly, however since we have a system of four linear equations with six unknow parameters:

$$
\begin{bmatrix} U_1 \\ U_2 \\ U_3 \\ U_4 \end{bmatrix} = \begin{bmatrix} 1 & 1 & 1 & 1 & 1 & 1 \\ k_r & -k_r & k_r & -k_r & k_r & -k_r \\ \frac{\sqrt{3}}{2} l_r & 0 & -\frac{\sqrt{3}}{2} l_r & -\frac{\sqrt{3}}{2} l_r & 0 & \frac{\sqrt{3}}{2} l_r \\ -\frac{1}{2} l_r & -l_r & -\frac{1}{2} l_r & \frac{1}{2} l_r & l_r & \frac{1}{2} l_r \end{bmatrix} \times \begin{bmatrix} T_1 \\ T_2 \\ T_3 \\ T_4 \\ T_5 \\ T_6 \end{bmatrix}. \tag{34}
$$

One way to solve this problem is to apply additional restrictions to the relative thrust values of the motors. These restrictions, however, should not limit the UAV's ability to perform motions along each axis independently. For example, we can state that the overall thrust $T_1 + T_4$ is equal to $T_3 + T_6$. Considering the location of the motors in Fig. 2, this restriction doesn't limit the motion of the hex-rotor.

For another restriction, we could perform heading rotation by changing the thrust (and thus rotation rate) of motors 2 and 5. Then, we can define both of these conditions as follows:

$$
\begin{cases} 0.5\left(T_1 + T_3 + T_4 + T_6\right) - \left(T_2 + T_5\right) = 0; \\ \left(T_1 + T_4\right) - \left(T_3 + T_6\right) = 0. \end{cases} \tag{35}
$$

Combining the systems (34) and (35) gives us a system of six equations with six unknowns. The analytical solution for this system takes the form:

$$
\begin{aligned}
T_1 &= \frac{l_r U_2 - k_r U_4 + \frac{\sqrt{3}}{2} k_r U_3 + k_r l_r U_1}{6 k_r l_r};\\
T_2 &= -\frac{2 k_r U_4 + l_r U_2 - k_r l_r U_1}{6 k_r l_r};\\
T_3 &= -\frac{-l_r U_2 + k_r U_4 + \frac{\sqrt{3}}{2} k_r U_3 - k_r l_r U_1}{6 k_r l_r};\\
T_4 &= \frac{-l_r U_2 + k_r U_4 - \frac{\sqrt{3}}{2} k_r U_3 + k_r l_r U_1}{6 k_r l_r};\\
T_5 &= \frac{2 k_r U_4 + l_r U_2 + k_r l_r U_1}{6 k_r l_r};\\
T_6 &= \frac{-l_r U_2 + k_r U_4 + \frac{\sqrt{3}}{2} k_r U_3 + k_r l_r U_1}{6 k_r l_r}.
\end{aligned}
\tag{36}
$$

Equations (36) allow us to calculate the thrust of each individual motor to achieve the desired UAV motion. It should be noted that in real systems, the control inputs are actually PWM signals for the motor controllers that correspond to the desired motor's rotation rate. Generally, the thrust generated by a motor is a function of its rotation rate squared, but in real applications, it also depends on the axial velocity across the rotor disk [6,11]. This aerodynamic effect should be taken into consideration when generating PWM signals for the motor controllers. For the purpose of this paper, we will stop at calculated thrust values and use them for simulation.

4 Results

In this section, the simulation results are presented. To test the performance of the suggested control method, we conducted a series of simulation tests with different flight conditions for hex-rotor aircraft. The simulation parameters are as follows: $m = 6$ kg; $l_r = 0.3$ m; $S_x = 0.03$ m^2; $S_y = 0.026$ m^2; $S_z = 0.0585$ m^2; $S_a = 0.04$ m^2; $k_r = 0.08$ m; $I_{ax} = I_{ay} = 0.02$ kg·m^2; $I_{az} = 0.03$ kg·m^2; $I_R = 3.06 \cdot 10^{-5}$ kg·m^2; $\rho = 1.2$ kg/m^3; $C_{Tx} = C_{Ty} = -0.8$; $C_{Tz} = -0.12$; $C_{Rx} = C_{Ry} = -0.05$; $C_{Rz} = -0.02$. The control parameters were derived experimentally: $k_2 = 2.4$ 1/s^2; $n_2 = 1.35$ 1/s; $k_4 = 2.4$ 1/s^2; $n_4 = 1.35$ 1/s; $k_6 = 4.65$ 1/s; $k_7 = k_9 = k_{11} = 3.15$ 1/s; $k_8 = 1.3$ 1/s; $k_{10} = 1.4$ 1/s; $k_{12} = 1.3$ 1/s; $k_{px} = 0.45$ 1/s; $k_{py} = 0.7$ 1/s; $k_{pz} = 1.3$ 1/s; $k_{ph} = 3.4$ 1/s; $k_{dx} = k_{dy} = k_{dz} = 0.1$; $k_{dh} = 0.2$. The maximum linear velocity of the UAV was restricted to 3 m/s during the simulation.

In the first test, we will use a very simple given trajectory, consisting of just 2 waypoints: (0, 0, 0, 0) and (20, 0, 20, 0). We will compare the results of the suggested approach (Fig. 5) and the stabilization control, described in [4] (Fig. 5).

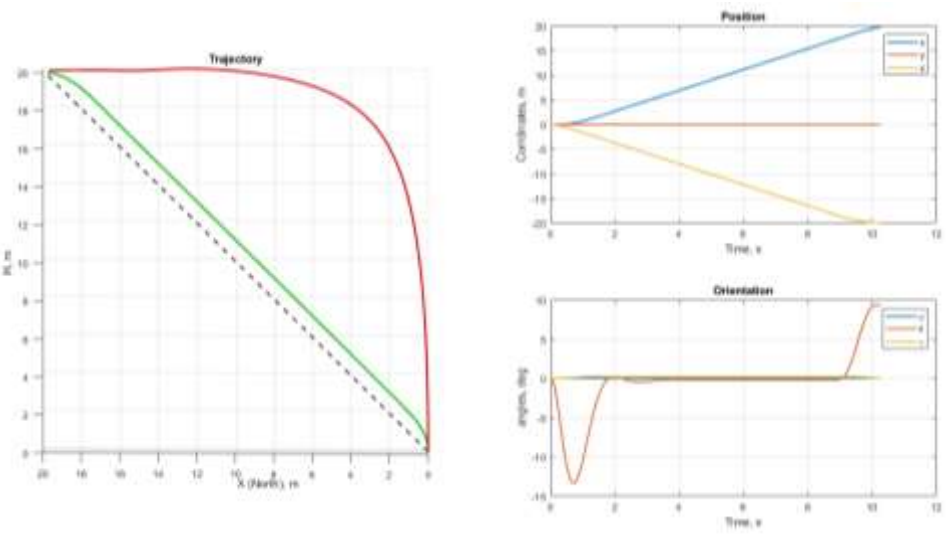

Fig. 5. The comparison results (UAV trajectory is presented on the left: green line indicates the results of the suggested approach; the red line indicates the results of stabilization control in [4]).

Obtained simulation results: for the suggested approach the mean trajectory offset is 0.2 m, the standard deviation – 0.42 m, and the maximum value is 1.13 m; for the stabilization control, the mean trajectory offset is 4.42 m, the standard deviation – 4.31 m, and the maximum value – 14.18 m.

For the second test, we will consider the performance of the suggested control approach with a more complex given trajectory that includes vertical take-off, horizontal flight, and slope landing. The trajectory parameters are: (0, 0, 0, 0), (0, 0, 30, 0), (100, 0, 30, 0), (120, 0, 0, 0). The results are presented in Figs. 6-7.

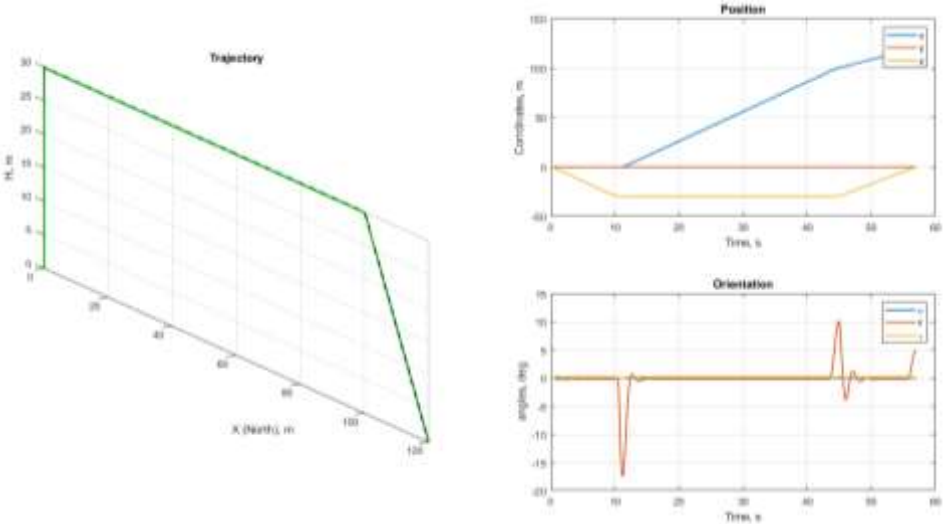

Fig. 6. The second test results: UAV's trajectory, position, and orientation.

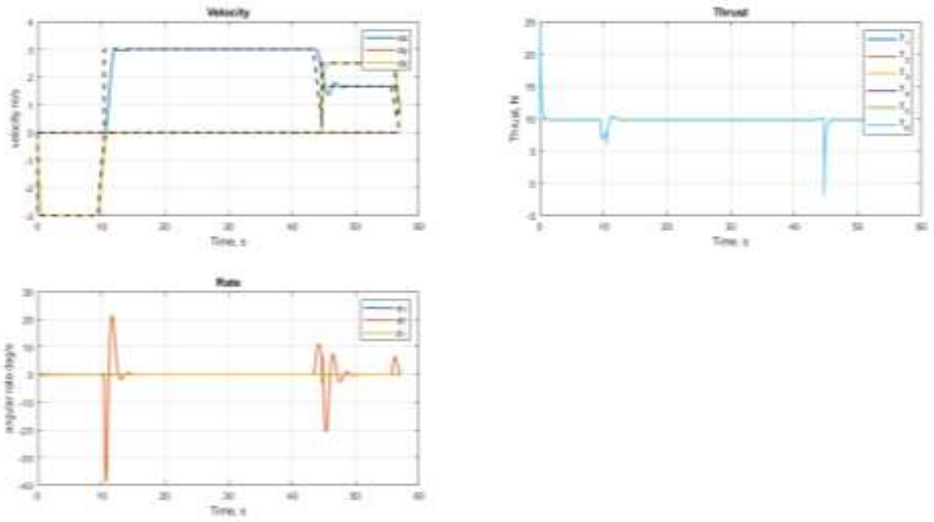

Fig. 7. The second test results: velocity, rotation rate, and thrust values.

In the second test, the mean trajectory offset was 0.9 m, the standard deviation – 0.022 m, and the maximum error value was equal to 0.42 m.

In the third simulation test, we will estimate the trajectory offset when the UAV is performing sharp turns in the horizon plane (Figs. 8,9). The given trajectory is as follows: (0, 0, 30, 0), (50, 0, 30, 0), (50, 50, 30, 0).

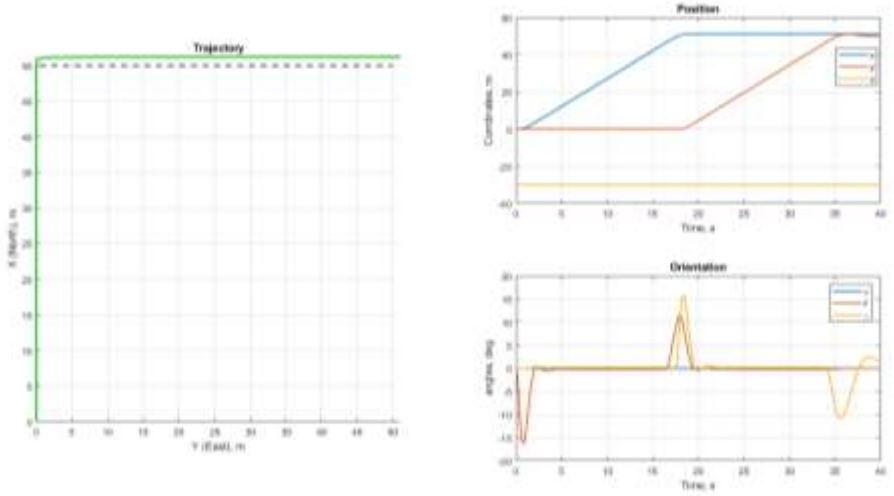

Fig. 8. The third test results: trajectory, position, and orientation.

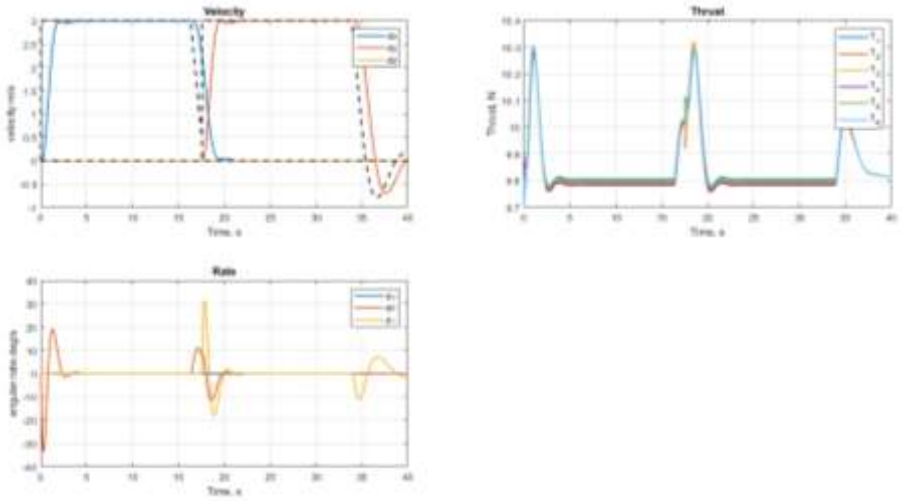

Fig. 9. The third test results: velocity, rotation rate, and thrust values.

In this test, the mean trajectory offset was 0.62 m, the standard deviation – 0.032 m, and the maximum error value was equal to 1.21 m.

For the fourth test, we will add UAV heading motion along the more complex given trajectory: (0,0,0,0), (80,20,30,0.78), (110,50,33,-0.52), (40,90,15,-0.78), (90,110,20,0.2), (0,0,0,0). The heading angle values are given in radians. The results are presented in Figs. 10-11.

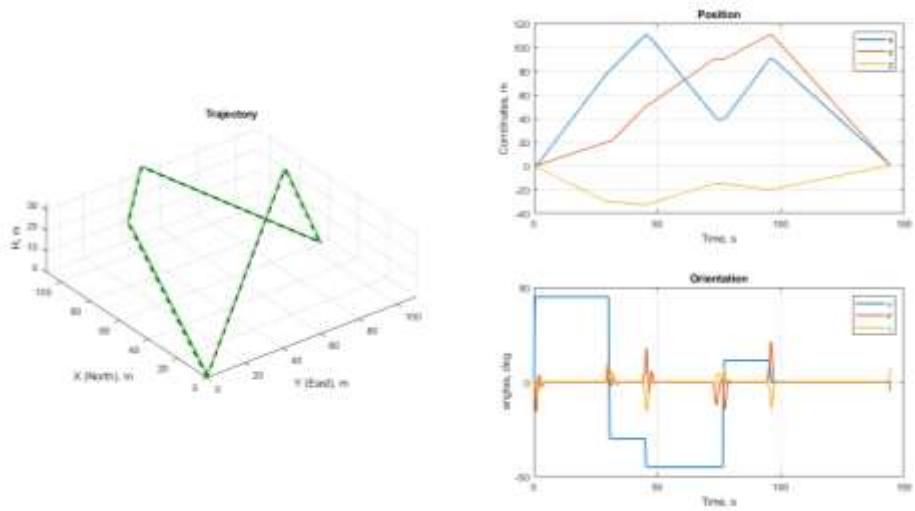

Fig. 10. The fourth test results: trajectory, position, and orientation.

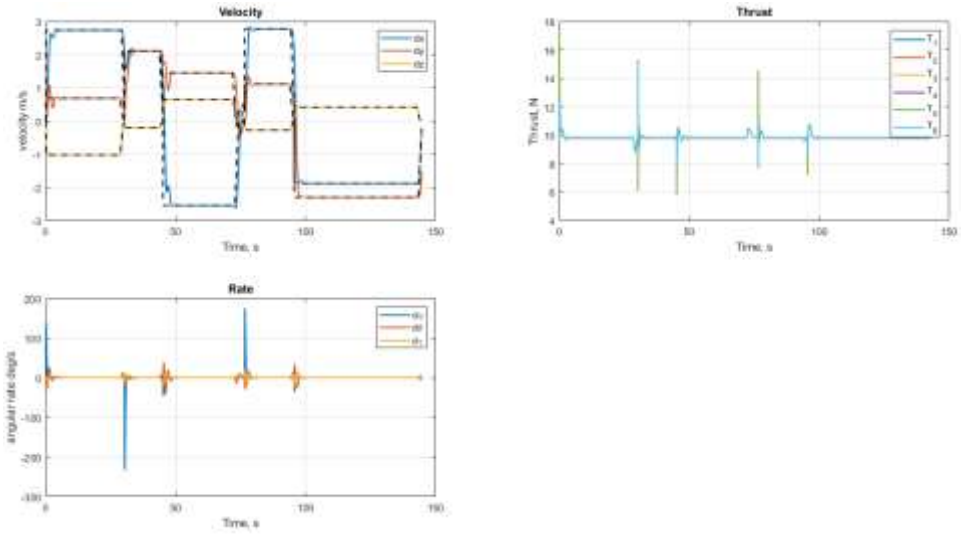

Fig. 11. The fourth test results: velocity, rotation rate, and thrust values.

The results of the fourth test: mean trajectory offset is 0.62 m, the standard deviation is 0.29 m, and the maximum value – 1.43 m.

And for the fifth and final simulation test, we will estimate the effect of control noise on the performance of the suggested approach. The control signal noise is added to the outputs of the trajectory control loop and is generated as Gaussian noise [12].

For this test, the following trajectory was used: (0,0,0,0), (0,0,30,-0.52), (50,0,30,0), (65,30,35,0.63), (50,60,30,0), (0,70,20,-0.45), (0,60,0,0). To reduce the impact of the statistical errors, we will perform this simulation 10 times (Fig. 12). During these simulation runs, noise signal mean values ranged from 1 to 8 percent, and std values ranged from 0.01 to 0.05 meters per second and 0.05 to 0.03 radians per second, respectively.

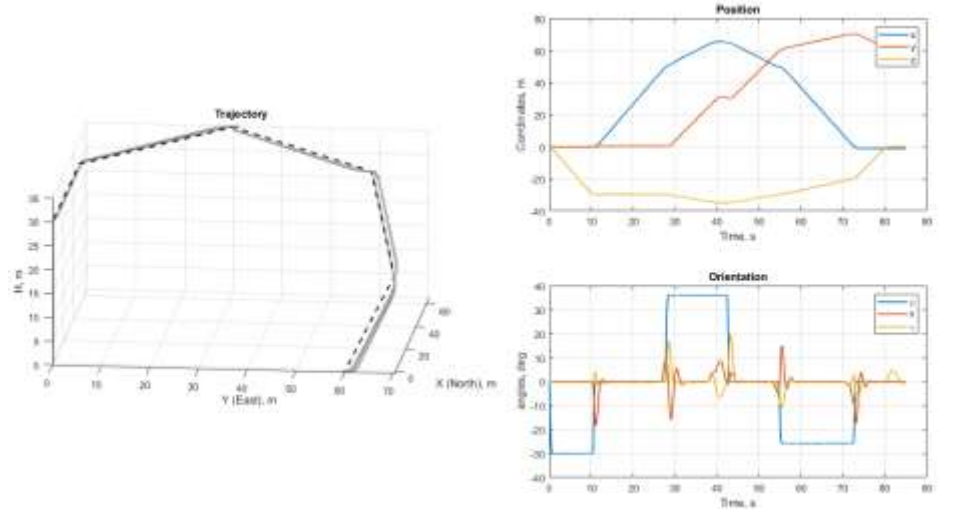

Fig. 12. The fifth test results: trajectory, position, and orientation (UAV trajectory during each of the simulation runs is indicated in grey colour).

The average results of the fifth test are: trajectory offset – 0.58 m, standard deviation – 0.26 m. Maximum offset across all tests – 1.31 m.

The provided simulation results prove that the proposed control method can minimize the trajectory offset. The details are discussed in the next section of this paper.

5 Discussion

Analyzing the results presented in Fig. 5, it is obvious that the proposed approach provides a much smaller trajectory offset. It should be noted, however, that in the work [4], the trajectory offset was never considered; the described approach provides asymptotic convergence of the UAV state-space vector to the given position coordinates. Another downside of this approach is that it doesn't allow for controlling UAV flight velocity, which might be crucial in some applications.

The second simulation scenario demonstrates that the approach proposed in this research is capable of generating stable control signals for any stage of UAV motion: vertical take-off, horizontal flight, and landing.

One of the concerns of the proposed control methodology is whether or not "headless" flight mode will generate significant trajectory overshoot during sharp turns since the complex dynamics of the UAV don't allow for a sudden stop along one axis with simultaneous acceleration along another. The simulation results presented in Figs. 8,9 prove that this effect really exists, but the value of overshoot in this simulation case reached only 1.21 m. which is still within the permitted interval.

The fourth simulation test proves that with a developed control system, the UAV is capable of flying along a complex semi-linear trajectory with simultaneous heading orientation changes. The maximum value of trajectory offset is 1.43 m and can be further reduced by fine-tuning control parameters.

The results of the final simulation test prove that the proposed control method is robust to internal noise in the trajectory loop output signals. The simulation was repeated ten times, and during those runs, the maximum value of the trajectory offset reached 1.31 m. The mean offset value across all tests equals 0.58 m. and the standard deviation is 0.26 m. According to these results, the UAV will stay within 1.36 meters of the given trajectory in 99.7% of cases. In all of the simulation scenarios, the maximum trajectory offset did not exceed 1.5 m.

6 Conclusion

In this paper, a trajectory control method for a hex-rotor UAV is proposed. This method is based on dividing the control process into two separate control loops: trajectory and locomotion control. The trajectory control loop generates the required linear velocities for the UAV as well as the required heading angular rate. It then applies restrictions to these values, specifically designed to minimize the trajectory offset error. Restricted values are then used as inputs for a locomotion control loop that is based on the Kokotovich approach to control synthesis. The locomotion loop generates the required thrust values for each motor to achieve the desired trajectory motion of the UAV. Provided thorough simulation results prove the effectiveness of the designed control system.

In follow-up research, optimal control parameters should be found, and a detailed comparison of the proposed method with commonly used control approaches should be provided.

The research was supported by RSF (project No. 23-29-00958).

References

1. Y. Lei, M. Cheng Aerodynamic, Appl. Sci. **9(22)**, 4797 (2019)
2. C. J. Zhao, Y. Bai, X. Gong, C. Peng, D. F. Xu, Z. J. Xu, Optics and Precision Eng. **23**, 1088-1095 (2015)
3. A. Alaimo, A. V. Artale, C. Milazzo, A. Ricciardello, J. of Int. and Rob. Syst. **73**, 261-270 (2014)
4. C. A. Arellano-Muro, L. F. Luque-Vega, B. Castillo-Toledo, A. G. Loukianov, "Backstepping control with sliding mode estimation for a hexacopter", in *10th Int. Conf. on Elec. Eng., Comp. Sci. and Automatic Control (CCE)* (2013), pp. 31-36
5. K. S. Lelkov, *Hex-rotor aircraft dynamics and simulation*, AIP Conf. Proc. **2948(1)**, 020015 (2023)
6. M. Bangura, M. Melega, R. Naldil, R. Mahony, *Aerodynamics of Rotor Blades for Quadrotors* (arXiv: Fluid Dynamics, 2016)
7. C. Zaibin, J. Hongguang, Complexity **2020**, 1-14 (2020)
8. G. Cai, B. Chen, T. Lee, *Coordinate Systems and Transformations*, Unmanned Rotorcraft Systems. Adv. in Ind. Control, (Springer, 2011)
9. D. Hamza, Z. Zoubir, *Comparative Study of PID, PD, LQR, and LQR-PD Regulators for Quadrotor Stabilization and Trajectory Tracking* (2023)
10. P. V. Kokotovic, IEEE Control Systems Magazine **12(3)**, 7–17 (1992)
11. A. Al, A. Dewi, T. Hidayat, MATEC Web of Conferences **215**, 01013 (2018)
12. L. Ding, H.-N. Wang, Z.-H. Guan, J. Chen, "Tracking Under Additive White Gaussian Noise Effect", in *Proc. of the 7th Asian Control Conf.* (2009), pp. 477-482